JOURNAL OF SOLID STATE CHEMISTRY **138,** 41–46 (1998)
ARTICLE NO. SC987752

Effect of Supported Na^+ Ions on the Texture Properties of ZrO_2

Zheng Liu, Weijie Ji, Lin Dong, and Yi Chen[1]

Department of Chemistry, Nanjing University, Nanjing 210093, People's Republic of China

Received June 17, 1997; in revised form December 8, 1997; accepted January 12, 1998

The dispersion of sodium nitrate on tetragonal zirconia and the effect of the dispersed sodium species on the textural properties of the support are investigated by using XRD, LRS, DTA, and BET surface area measurement. The results indicate that $NaNO_3$ can be dispersed on the surface of tetragonal zirconia by the incorporation of Na^+ ions into the surface vacant sites. The experimentally measured dispersion capacity of sodium nitrate on t-ZrO_2 is consistent with the value deduced from the incorporation model, i.e., 8.6 Na^+/nm^2t-ZrO_2. The dispersed Na^+ ion species can effectively hinder the sintering of zirconia and prevent its phase transformation from tetragonal to monoclinic. The crystallization temperature and surface area of the samples are strongly dependent on the loaded amount of $NaNO_3$ when it is below the dispersion capacity. Crystalline $NaNO_3$ is detected when its loading exceeds the dispersion capacity and has less effect on the structural and textural properties of the t-ZrO_2.

Key Words: **tetragonal zirconia; sodium; texture; dispersion; incorporation model.**

INTRODUCTION

Interaction between metal compounds and supports has attracted much attention because of the wide applications of supported-metal compound systems and has been discussed in several papers (1–3) that assume metal cations are incorporated or penetrate into the surface layer or the bulk phase of the support. The incorporation model proposed by Chen *et al.* has suggested that the dispersed metal cations are incorporated into surface vacant sites of the support, with their accompanying anions positioned on the top for extra charge compensation. Dispersion capacities of some metal oxides and halides on γ-Al_2O_3 and CeO_2 derived by the model are in good agreement with the experimental results (4–7).

Zirconia, a versatile ceramic material of great technical interest, has found wide practical or potential applications, e.g., it is a promising category of catalyst or catalyst support for some important chemical synthesis industries, due to its excellent mechanical, electronic, and optical properties (8–13). Several metal oxide–zirconia systems have already been the subject of study (14–16).

Zirconia exhibits three polymorphic forms, the monoclinic (m), tetragonal (t), and cubic (c) phases. Although the monoclinic phase is thermodynamically more stable, the tetragonal form can be stabilized at room temperature under certain conditions. It has been reported that tetragonal zirconia (t-ZrO_2) can be stabilized by introducing some metal cations, e.g., V^{4+} (15), Mo^{6+} (17), and Y^{3+} (18, 19). Recently, studies have been devoted to the interaction between the doped metal cations and zirconia (14, 15, 17). Cimino and co-workers demonstrated that a high-surface-area t-ZrO_2 can be obtained by impregnating hydrous zirconia with Cr^{6+} solution; the supported Cr^{6+} species prevent the phase transition from tetragonal to monoclinic (14). So far, attention has mainly focused on transition-metal compounds, and only a few studies consider the effects of alkali-metal compounds (20, 21).

Alkali promoters are often used to improve catalytic activity or selectivity in industrial supported catalysts. It seems reasonable that the interaction between the alkali promoter and the support should have a major impact upon the influence of the promoter on the dispersion and reducibility of the active component, which is obviously important in modifying the catalytic behaviour of the catalyst (22). In this paper, the interaction between $NaNO_3$ and the zirconia support is studied using X-ray diffraction (XRD), differential thermal analysis (DTA), laser Raman spectroscopy (LRS), and BET surface area measurements. Special attention is given to the dispersion behaviour of sodium species on tetragonal zirconia and the effect of the dispersed species on the textural properties of zirconia.

EXPERIMENTAL

Materials

Hydrous zirconia was prepared by rapid addition of concentrated NH_4OH into a $ZrOCl_2 8H_2O$ (A. R.) aqueous solution (0.3 M) to produce a suspension with a pH value of about 10.5. The precipitate was washed with distilled water

[1]To whom correspondence should be addressed.

0022-4596/98 $25.00

to pH 7 with no detectable Cl^- and then dried at 373 K for 10 h.

Tetragonal ZrO_2 support was prepared following the procedures reported in the literature (23). In particular, sodium hydroxide solution (4 M) was added to the above suspension until pH $\geq$ 14; the precipitate was washed with distilled water to pH 7 with no detectable Cl^- and then dried at 373 K for 10 h. The dried sample calcined at 773 K for 4 h had a BET surface area of 60 m^2/g. LRS and XRD measurements proved that the calcined ZrO_2 samples were tetragonal zirconia.

Samples with different Na^+ ion content were prepared by two methods: (i) incipient wetness impregnation of hydrous zirconia powder with an aqueous solution of $NaNO_3$ followed by calcination at 773 K for 2 h in flowing air; (ii) impregnation of tetragonal ZrO_2 with an aqueous solution of $NaNO_3$.

Characterization

BET surface areas were measured by nitrogen adsorption at 77 K on a Micrometrics ASAP-2000 adsorption apparatus.

Differential thermal analysis (DTA) was carried out from room temperature to 1073 K (heating rate 10 K min^{-1}) using a Rigaku TG-DTA thermoanalyzer in flowing air.

X-ray powder diffraction patterns were collected with a Shimadzu XD-3A diffractometer using Ni-filtered Cu$K\alpha$ radiation (0.15418 nm). The X-ray tube was operated at 35 kV and 15 mA.

Raman spectra were recorded on a Bruker RFS-100 spectrometer with a wave number accuracy of 4 cm^{-1}. The samples were measured in powder form, and a Na: YAG crystal laser was used for excitation.

Related physical parameters of samples as prepared are listed in Table 1.

TABLE 1
Physical Properties of Samples

Sample[a]	Content of $NaNO_3$ (wt. % $NaNO_3/ZrO_2$)	Content of $NaNO_3$ (Na^+/nm^2)	BET surface area (m^2/g)
N_1Z(I)	3.0	4.6	45.4
N_2Z(I)	6.0	7.4	58.3
N_3Z(I)	8.7	9.8	62.1
N_4Z(I)	25	—	20.2
N_5Z(I)	51	—	10.5
N_1Z(II)	6.7	7.9	
N_2Z(II)	8.5	10	
N_3Z(II)	15.4	18.2	
N_4Z(II)	34.0	40.1	
N_5Z(II)	51.0	60.2	

[a]N: $NaNO_3$, Z: ZrO_2, (I) and (II) designate (i) and (ii) in the preparation methods, respectively.

RESULTS AND DISCUSSION

The Dispersion of Na^+ Species on t-ZrO_2

Since conventional XRD technique is not sensitive enough to detect very small crystalline particles and our XRD profiles (Fig. 1B) cannot clearly discriminate the crystalline forms of t-ZrO_2 and c-ZrO_2, LRS is used to identify the crystalline form of the support as well as to monitor the dispersion of $NaNO_3$ on it. As shown in Fig. 1A, the 643, 463, 269, and 148 cm^{-1} Raman peaks of the zirconia support are consistent with the characteristic peaks of tetragonal zirconia, t-ZrO_2 (21, 24–26). The weak shoulder peak around 610 cm^{-1} coexisting with the above peaks has also been attributed to the contribution of t-ZrO_2 (24, 25), although it has been reported that c-ZrO_2 gives only a single broad peak around 610 cm^{-1} in the 100–700 cm^{-1} region (24, 25). The XRD profile of the same support in Fig. 1B shows an asymmetric peak around $2\theta = 35°$. This peak is broader (with half-width about 0.7°) than the main peak around $2\theta = 30°$ (half-width about 0.4°). Although the peak of t-ZrO_2 at $2\theta = 34°$ has not been detected, the combination of the above LRS and XRD results leads to the conclusion that the support as prepared is predominately in the

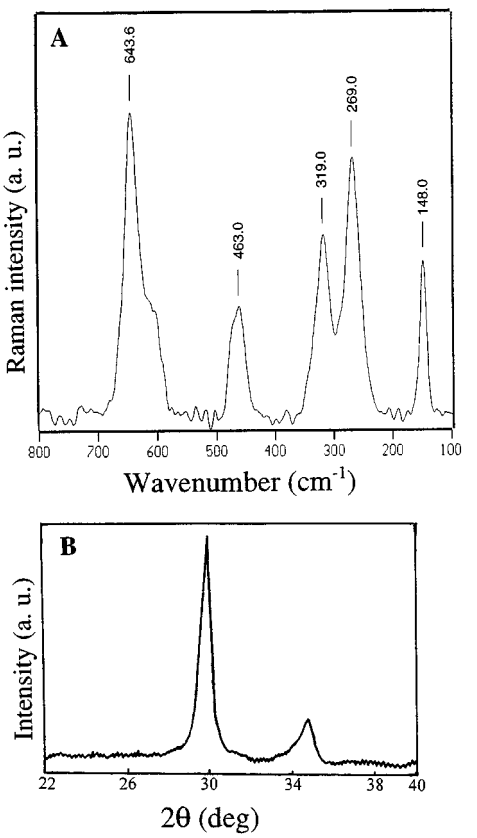

FIG. 1. (A) Raman spectrum and (B) XRD pattern of t-ZrO_2 as support calcined at 773 K.

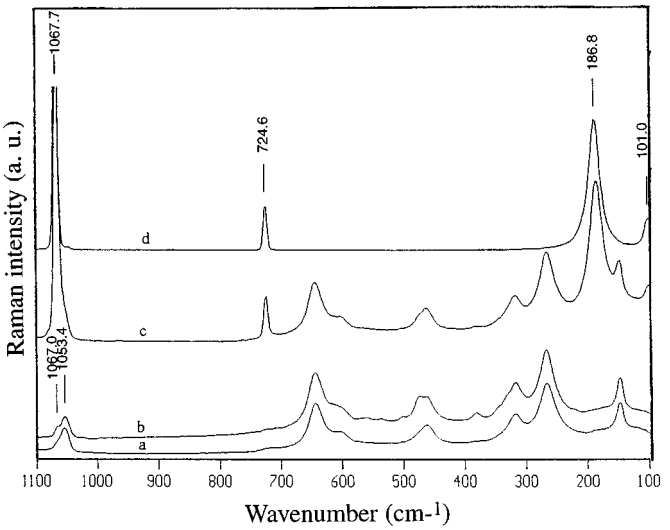

FIG. 2. Raman spectra of samples calcined at 773 K. a: $N_1Z(II)$; b: $N_2Z(II)$; c: $N_3Z(II)$; d: pure $NaNO_3$.

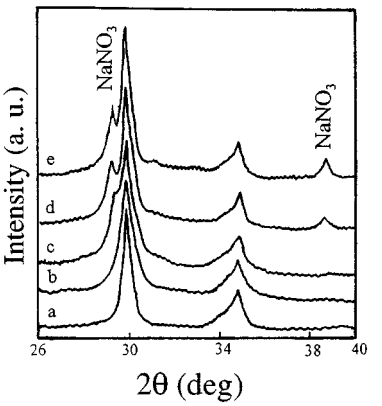

FIG. 3. XRD patterns of samples calcined at 773 K for 1 h. a: $N_1Z(II)$; b: $N_2Z(II)$; c: $N_3Z(II)$; d: $N_4Z(II)$; e: $N_5Z(II)$.

form of t-ZrO_2 with no appreciable amount, if any, of c-ZrO_2.

The Raman spectra of samples with various loading amounts of $NaNO_3$ are shown in Fig. 2, with pure $NaNO_3$ listed for comparison. For the sample with 7.9 Na^+/nm^2 (Fig. 2a), in addition to the Raman bands of the support and the new band at 1053.4 cm^{-1} are tentatively ascribed to the surface $NaNO_3$ species strongly interacting with the zirconia. With the increase of the loading of $NaNO_3$, another band at 1067.7 cm^{-1} appears in Figs. 2b and 2c, indicating the existence of bulk-phase $NaNO_3$ in those samples, in contrast to the Raman spectrum of $NaNO_3$ (Fig. 2d).

The above results suggest that there are two forms of supported $NaNO_3$ species on the surface of zirconia: the surface species strongly interacting with the support and the bulk-like species less influenced by zirconia. From the above results, the $NaNO_3$ dispersion capacity of 7.9–10 Na^+/nm^2 on t-ZrO_2 is estimated.

The XRD profiles of the same series of samples are shown in Fig. 3. No bulk-phase $NaNO_3$ has been detected in the sample with 7.9 Na^+/nm^2 (Fig. 3a), indicating that in this case $NaNO_3$ is highly dispersed on the surface of the support. As can be seen from Figs. 3b–3e, the intensities of the peaks corresponding to bulk-phase $NaNO_3$ increase with the increase of the loading amount of sodium nitrate. The results are consistent with those obtained from LRS.

To investigate the effect of calcination temperature on the interaction between $NaNO_3$ and ZrO_2 and the stability of the samples, the XRD patterns of the $N_5Z(II)$ sample (60.2 Na^+/nm^2) calcined at various temperatures are shown in Fig. 4. The intensities of the diffraction peaks of bulk-phase $NaNO_3$ decrease dramatically from 393 to 623 K and then remain unchanged with the further increase of the temperatures to as high as 813 K. The results indicate that appropriate calcination temperature is necessary to promote the dispersion of $NaNO_3$ on t-ZrO_2. In addition, the sample is stable after being calcined at 773 K for 2 h (Fig. 4d) or even at 813 K for 1 h (Fig. 4e).

The DTA results are presented in Figure 5. The two endothermic peaks at 576 and 975 K for the pure $NaNO_3$ sample (Fig. 5f) are attributed to the melting and decomposition of bulk sodium nitrate, respectively. The features of the DTA profiles of the supported samples are dependent on the loading amount of sodium nitrate. Apparently, no endothermic peaks similar to these two can be observed when the loadings are relatively low, as shown in Figs. 5a and 5b for samples with Na^+ loading of 7.9 and 10 Na^+/nm^2, respectively. The loading amount of sodium nitrate in the above two samples was lower than or close to the dispersion capacity of sodium nitrate on t-ZrO_2. Similar results for $LiNO_3$ supported on γ-alumina samples have been obtained

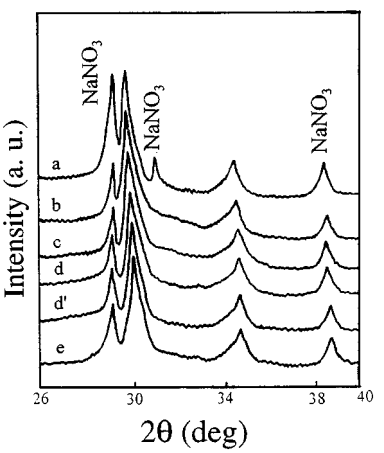

FIG. 4. XRD patterns of sample $N_5Z(II)$ calcined at varying temperatures. a: 393 K (4 h); b: 623 K (1 h); c: 723 K (1 h); d: 773 K (1 h); d′: 773 K (2 h); e: 813 K (1h).

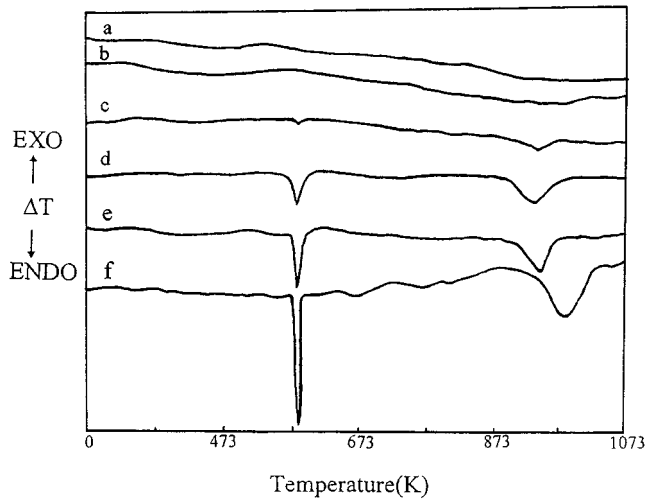

FIG. 5. DTA curves of the samples before calcination. a: $N_1Z(II)$; b: $N_2Z(II)$; c: $N_3Z(II)$; d: $N_4Z(II)$; e: $N_5Z(II)$; f: $NaNO_3$.

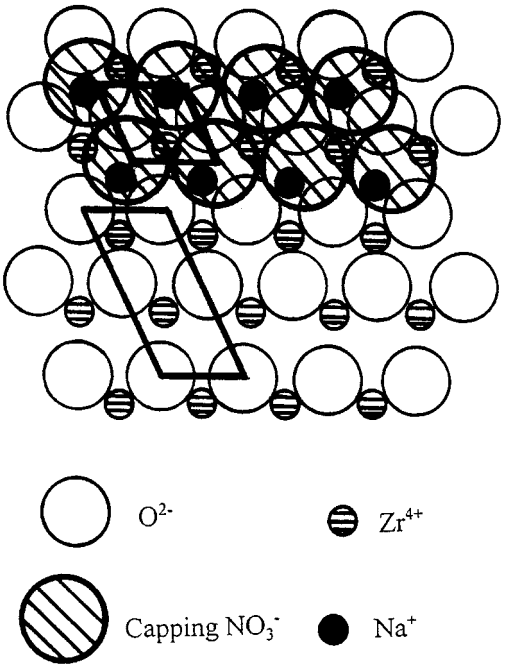

FIG. 6. A tentative model of the surface $NaNO_3$ formed on the (111) plane of t-ZrO_2.

in our lab under N_2 atmosphere with the same heating rate. An endothermic peak corresponding to the decomposition of the dispersed lithium nitrate has been observed for a sample with $LiNO_3$ loading around 6.5 Li^+/nm^2 (7). The absence of the decomposition endothermic peak in the above two samples might be due to the strong interaction of the highly dispersed $NaNO_3$ with t-ZrO_2, although there is a possibility that the endothermic effects of these two samples are too low to be detected by DTA. For samples with loadings beyond the dispersion capacity, the decomposition temperature of $NaNO_3$ remains almost unchanged in the range 936–942 K.

The above LRS, XRD, and DTA results point out that $NaNO_3$ can be highly dispersed on the surface of t-ZrO_2, with a dispersion capacity of around 7.9–10 Na^+/nm^2.

It has been suggested that the low index (111) plane is preferentially exposed on the surface of t-ZrO_2, and this plane has been reported as being identified with virtually no ambiguity by HRTEM (high resolution transmission electron microscopy) (27, 28). As shown in Fig. 6, one can estimate that there are two vacant sites in each unit mesh (approximately 0.23 nm^2) corresponding to a vacant site density of $\sim 8.6/nm^2$. According to the incorporation model, Na^+ ions can incorporate into the surface vacant sites of the support with the accompanying anion groups positioning on the top of the occupied sites for charge compensating. Taking 0.066 nm as the oxygen covalent radii and 0.12 nm as the N–O bond length (29), the size of the NO_3^- group is estimated to be around 0.11 nm^2, which is approximately half of a unit mesh on the (111) plane. Thus the capping NO_3^- group will not produce any shielding effect to prevent the vacant sites from being occupied by Na^+ ions. Accordingly, the dispersion capacity of $NaNO_3$ is calculated to be 8.6 Na^+/nm^2, which is consistent with the experimental results mentioned above. A tentative model for the incorporation of $NaNO_3$ on t-ZrO_2 with a loading amount below its dispersion capacity is also depicted in Fig. 6.

In light of the structure of the dispersion $NaNO_3$ species, as can be seen from Fig. 6, the interaction between the capping NO_3^- anions and their nearest-neighbor Zr^{4+} cations is also inevitable. As a result, these interactions might lead to the distortion of the anion groups, which might account for the presence of the Raman band at 1053.4 cm^{-1}. After all the available surface vacant sites have been occupied, the continued increase of the loading of $NaNO_3$ would lead to the formation of bulk-phase $NaNO_3$ on the support, identified by its characteristic Raman band at 1067.7 cm^{-1} (cf. Fig. 3).

The Effect of Dispersed Na^+ Species on the Texture of ZrO_2

Reported in Fig. 7A are the X-ray diffraction patterns of samples prepared by the impregnation of powder hydrous zirconia with varying amounts of $NaNO_3$ from an aqueous solution after calcination at 753 K. For all samples, the crystalline peaks of ZrO_2 are weak and broad, indicating the poor crystallization of zirconia. When the calcination temperature is increased to 773 K, the samples are better crystallized, as can be seen in Fig. 7B. Interestingly, a small amount of m-ZrO_2 coexisting with the tetragonal zirconia has been detected in the samples with $NaNO_3$ loading amount lower than dispersion capacity, and the intensity of

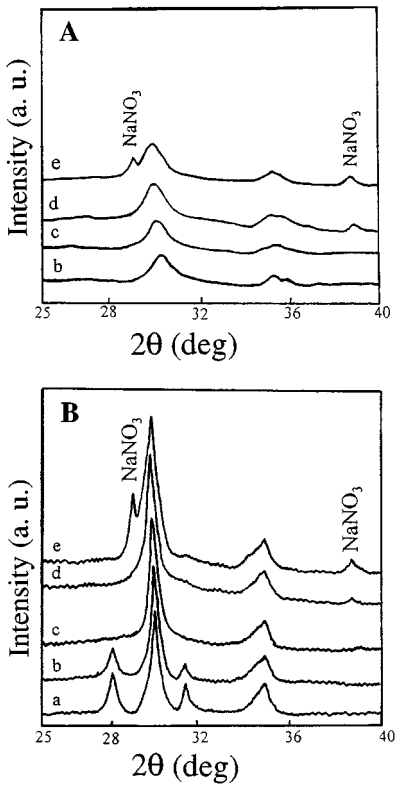

FIG. 7. XRD patterns of samples calcined at (A) 753 K and (B) 773 K. a: $N_1Z(I)$; b: $N_2Z(I)$; c: $N_3Z(I)$; d: $N_4Z(I)$; e: $N_5Z(I)$.

the m-ZrO_2 peaks gradually decreases with the increase of $NaNO_3$ loading (Figs. 7B(a) and 7B(b)). When Na^+ loading exceeds dispersion capacity, around 9.8 Na^+/nm^2, only t-ZrO_2 is detected. Finally, bulk-phase $NaNO_3$ is observed with the further increase of $NaNO_3$ loading. Apparently the stability of t-ZrO_2 has been improved by the addition of sodium nitrate. The stabilization effect is enhanced by the increase of the amount of Na^+ cations incorporated until all the available vacant sites are occupied.

It has been argued that the crystal form (tetragonal or cubic phase) of Na^+-stabilized zirconia has been fraught with controversy (21, 30). Raman measurements have been carried out to clarify the crystal form of the zirconia in the above samples calcined at 773 K. Typical results are shown in Fig. 8. The spectroscopic features in the range 700–1100 cm^{-1} are basically the same as in those samples prepared by the impregnation of t-ZrO_2 with $NaNO_3$ from an aqueous solution and calcined at 773 K. However, for the low loading sample (Fig. 8a) two small but rather sharp bands at 183 cm^{-1} and 193 cm^{-1} corresponding to m-ZrO_2 phase (25) have been observed in addition to surface $NaNO_3$ species (1053.4 cm^{-1}). The above two bands disappeared when the loading of $NaNO_3$ increased to about 9.8 Na^+/nm^2, with only t-ZrO_2 phase existing. These results are consistent with the XRD results discussed in the above section.

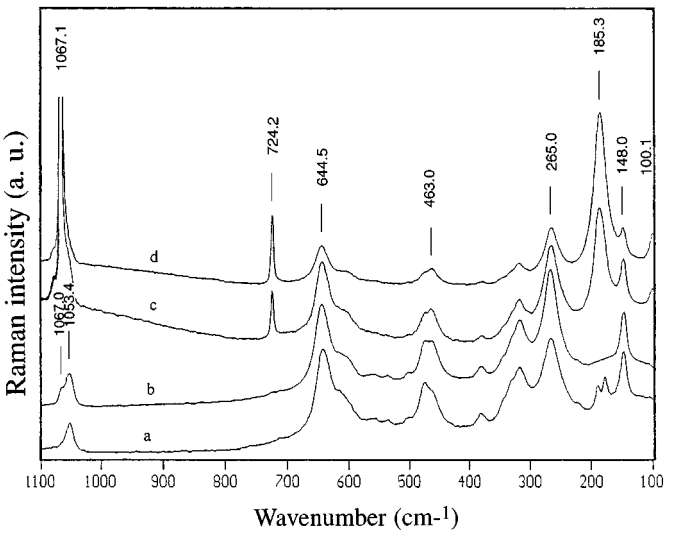

FIG. 8. Raman spectra of samples calcined at 773 K. a: $N_2Z(I)$; b: $N_3Z(I)$; c: $N_4Z(I)$; d: $N_5Z(I)$.

The stabilization effect exerted by the incorporated Na^+ should be related to the crystallization process of zirconia. It is claimed that amorphous hydrous zirconia contains very small regions in the form of platelets, and its structure is very similar to that of the (111) plane of tetragonal zirconia (27). Tani *et al.* (31) proposed that the presence of tetragonal-like ZrO_2 nuclei in amorphous zirconia would result in the formation of t-ZrO_2 at relatively low temperatures. It has been mentioned that if held at high temperature for a long period of time, t-ZrO_2 phase will always undergo phase transformation to m-ZrO_2, and this process will start at the particle surface and continue toward the centre of the crystal (27). Therefore, it is reasonable to consider that for the samples prepared by impregnation of amorphous hydrous zirconia with $NaNO_3$ from aqueous solution, Na^+ species might start incorporating into surface vacant sites as soon as the t-ZrO_2 phase is formed during calcination. The incorporated Na^+ cations bring about the separation of small zirconia particles, resulting in the decrease of the surface energy of the particles and the improvement of the stability of t-ZrO_2. When the content of $NaNO_3$ is relatively low, the phase transformation from t-ZrO_2 to m-ZrO_2 still can occur since part of the surface vacant sites on t-ZrO_2 have not been occupied. When the amount of $NaNO_3$ is close to its dispersion capacity, the full occupation of the surface vacant sites prevents the phase transformation of t-ZrO_2 to m-ZrO_2 from occurring, and only tetragonal zirconia is formed. Moreover, the stabilizing effect of Na^+ ions on tetragonal zirconia also results in the increase of the surface area of the samples. As can be seen from Table 1, such effect is most significant when the content of $NaNO_3$ is close to its dispersion capacity, as in sample $N_3Z(I)$ (62m^2/g).

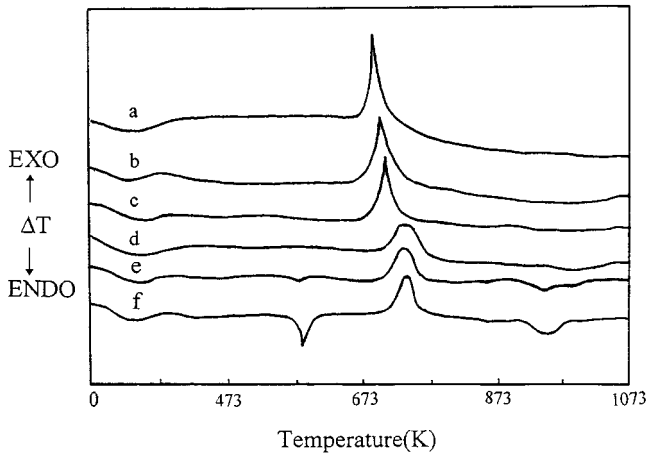

FIG. 9. DTA curves of precursors of samples. a: ZrO_2; b: $N_1Z(I)$; c: $N_2Z(I)$; d: $N_3Z(I)$; e: $N_4Z(I)$; f: $N_5Z(I)$.

It has been reported that the crytallization temperature of amorphous zirconia starts at about 697 K (32). Our experimental results indicate that the $NaNO_3$-containing hydrous zirconia is not fully crystallized even after calcination at 753 K, as shown in Fig. 7A. The DTA profiles listed in Fig. 9 show that the crystallization of zirconia is delayed due to the presence of $NaNO_3$ species. The sharp exothermic peak at around 697 K resulting from the crystallization of hydrous zirconia (32) shifts to higher temperatures with the presence of highly dispersed Na^+ cations, i.e., from 697 K for pure hydrous zirconia to $\sim$741 K for the sample with Na^+ loading of 9.8 Na^+/nm^2. Moreover, when the content of $NaNO_3$ exceeds its dispersion capacity the temperature shift is no longer observed, indicating that further increase of Na^+ content has little effect on the crystallization of the zirconia.

CONCLUSION

$NaNO_3$ can be dispersed on the surface of tetragonal zirconia through the incorporation of Na^+ cations into the surface vacant sites, and its dispersion capacity quantitatively evaluated by the incorporation model, i.e., 8.6 Na^+/nm^2, is consistent with the results determined by LRS and XRD. Crystalline $NaNO_3$ is observed only when the loading amount is higher than the dispersion capacity. The experimental results reveal that due to the interaction of the dispersed $NaNO_3$ with the surface of the tetragonal zirconia, the phase transformation from t-ZrO_2 to m-ZrO_2 is inhibited, and the surface area of the t-ZrO_2 produced by the calcination of hydrous zirconia is increased.

REFERENCES

1. M. L. Jacono, M. Schivaveuo, and A. Cimino, *J. Phys. Chem.* **75,** 1044 (1971).
2. M. Wu and D. M. Hercules, *J. Phys. Chem.* **83,** 2003 (1979).
3. B. Delmon and M. Houalla, *in* "Preparation of Catalysts (II)" (B. Delmon, P. Grang, P. A. Jacobs, and G. Poncelet, Eds.), p. 447. Elsevier, Amsterdam, 1979.
4. Y. Chen, L. F. Zhang, J. F. Lin, and Y. S. Jin, *in* "Catalytic Science and Technology" (S. Yshida, N. Takezawa, and T. Ono, Eds.), Vol. 1, p. 29. Kodansha, Tokyo, 1991.
5. Y. Chen and L. F. Zhang, *Catal. Lett*. **12,** 51 (1992).
6. Y. Chen, *et al*., *in* "Studies in Surface Science and Catalysis" (J. W. Hightower, W. N. Delgass, E. Iglesia, and A. J. Bell, Eds.), Vol. 101, p. 1293. Elsevier Science, Baltimore, 1996.
7. L. F. Zhang, J. F. Lin, and Y. Chen, *J. Solid State Chem.* **97,** 292 (1992).
8. A. H. Heuer and L. W. Hobbs, *in* "Advance in Ceramics", Vol. 3. Amer. Ceram. Soc., Columbus, OH, 1981.
9. D. Gargnli and D. Kunder, *J. Mater. Sci. Lett*. **3,** 503 (1984).
10. L. L. Hench and D. R. Ulrich, *in* "Ultrastructure Processing of Ceramic, Glasses, and Composites." Wiley–Interscience, New York, 1984.
11. B. Denise and R. P. A. Sneeden, *Appl. Catal.* **28,** 235 (1986).
12. Y. Amenomiya, *Appl. Catal*. **30,** 57 (1987).
13. H. Miyata, M. Kohno, T. Ohno, and F. Hatayama, *J. Mol. Catal.* **63,** 181 (1990).
14. A. Cimino, *et al*., *J. Catal.* **127,** 744 (1991).
15. J. R. Sohn, G. Cho, Y. Pate, and S. Hyashi, *J. Catal.* **159,** 170 (1996).
16. K. Q. Chen, Y. N. Fan, Z. Hu, and Q. J. Yan, *J. Mater. Chem.* **6,** 1041 (1996).
17. B. Y. Zhao, H. R. Ma, and Y. Q. Tang, *J. Catal.* (*China*) **16,** 171 (1995).
18. N. M. Gokhale, R. Dayal, S. C. Sharma, and Ramjilal, *J. Mater. Sci.* **29,** 5709 (1994).
19. M. Vrinat, D. Hamon, M. Breysse, B. Durand, and T. des Courieres, *Catal. Today* **20,** 273 (1994).
20. S. Sugigama, K. Shimodan, H. Hayashi, N. Shigemoto, K. Miyaura, K. Seitoh, and J. B. Moffot, *J. Catal.* **141,** 279 (1993).
21. G. Fagherazzi, P. Canton, A. Benedetti, F. Pinna, G. Mariotto, and E. Zanghellini, *J. Mater. Res.* **12,** 318 (1997).
22. T. E. Hoost and J. G. Goodwin, Jr., *J Catal.* **130,** 283 (1991).
23. W. Li, W. Z. Zhang, and Y. Q. Yin, *in* "7th National Conference on Catalysis (China)," p. 364. Dalian, 1994.
24. J. G. Cai, Y. S. Raptis, and E. Anastassakis, *Appl. Phys. Lett*. **62,** 2781 (1993).
25. T. Hirata, E. Asari, and M. Kitajima, *J. Solid State Chem.* **110,** 201 (1994).
26. A, Feinberg and C. H. Perry, *J. Phys. Chem. Solids* **42,** 513 (1981).
27. J. R. Anderson, *in* "Structure of Metallic Catalysts," p. 62. Academic Press, New York, 1975.
28. C. Morterra, G. Cerrato, and L. Ferroni, *Mater. Chem. Phys.* **37,** 243 (1994).
29. John Emsley, *in* "The Elements," p. 136. Clarendon Press, Oxford, 1991.
30. R. Srinivasan, S. F. Simpson, J. M. Harris, and B. H. Davis, *J. Mater. Sci. Lett*. **10,** 352 (1991).
31. E. Tani, M. Yoshimura, and S. Somiya, *J. Mater Sci. Lett*. **66,** 11 (1983).
32. C. J. Norman, P. A. Goulding, and I. Mcalpine, *Catal. Today* **20,** 313 (1994).